Combining burial history and rock-physics modeling to constrain AVO analysis during exploration

Per Avseth[1, 2] and Ivan Lehocki[3]

Abstract

We use combined burial history and rock-physics modeling of sand and shale to predict expected amplitude variation with offset (AVO) signatures and seismic fluid sensitivities for a given burial history. The advantage with this approach is that we can extrapolate away from wells in areas with complex tectonics. Furthermore, we can use depth trends derived from local burial history to create AVO probability density functions (PDFs) for calibration and classification of AVO attributes in a given area. We demonstrate the use of these techniques on two hydrocarbon discoveries with different burial histories: the Alvheim Field in the North Sea and the Skalle Field in the Barents Sea.

Introduction

Present-day rock-physics properties and associated seismic signatures are affected strongly by burial history, including mechanical compaction, diagenetic alterations, and tectonic events. Hence, to fully understand the seismic signatures of a hydrocarbon prospect, we should honor the geologic processes through time. Taking into account diagenesis and tectonic events, we can predict compaction trends and associated seismic velocities in areas with more complex burial history involving both mechanical and chemical compaction, as well as uplift episodes and corresponding erosion. The resulting rock-physics trends help us better understand expected seismic contrasts for a given prospect and better evaluate the potential to discriminate hydrocarbons from seismic amplitude variation with offset (AVO) data. The resulting trends can also be used to constrain AVO inversion and classification in areas with complex burial history.

Helset et al. (2004) were the first to combine kinetic modeling of quartz cementation and associated porosity evolution, introduced by Walderhaug (1996), with rock-physics modeling using contact cement theory by Dvorkin and Nur (1996). Brevik et al. (2011), Dræge et al. (2014), and Avseth et al. (2014) further showed how burial history can be combined with rock physics to improve the understanding of seismic signatures in areas with complex tectonics or in frontier areas with limited well control. In this study, we utilize this integrated approach to predict sandstone texture and associated seismic properties as a function of geologic time for a North Sea case and a Barents Sea case. The burial history of these two are very different, as the Barents Sea has been exposed to major tectonic uplift episodes, in particular in the Cenozoic (see Figure 1). We also model the properties of shales as a function of geologic time and burial history. This allows us to predict AVO signatures as a function of burial history, which is one of this study's main goals. Finally, we apply this methodology to create training data or AVO probability density functions (PDFs) for target intervals in both the North Sea and Barents Sea cases, which we use to classify real AVO data from the same areas and target intervals.

AVO modeling constrained by burial history

Step 1: Compaction modeling of sands and shales. First, we perform modeling of mechanical compaction and diagenesis of sands and shales as a function of burial history. Mechanical compaction is handled via empirical relationships between porosity and burial depth (Avseth et al., 2005). The porosity-decrease rate for sands and shales is more rapid at shallow depths and slows at greater

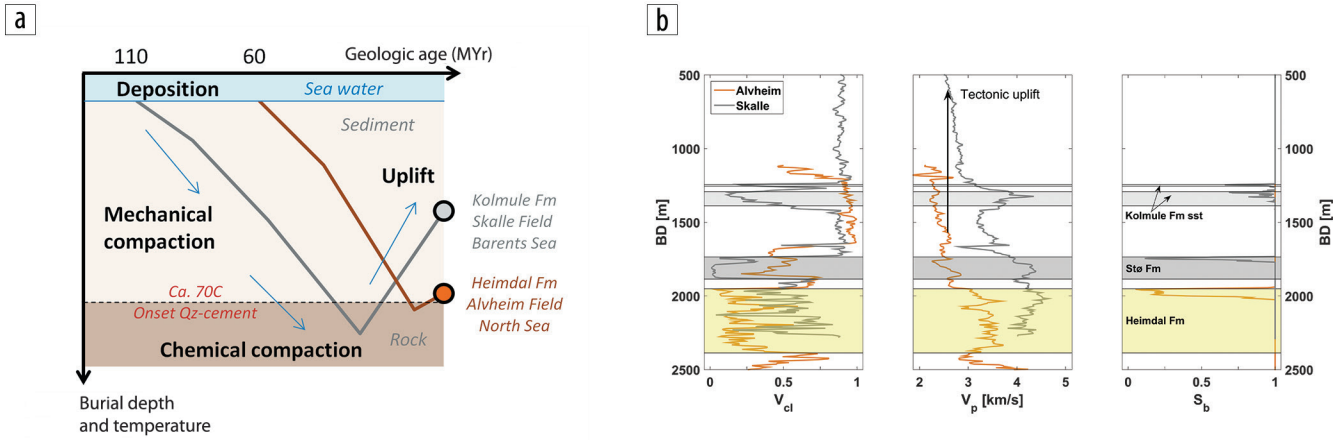

Figure 1. (a) Schematic burial history and (b) log profiles of two selected North Sea and Barents Sea wells with hydrocarbon discoveries. The logs are plotted versus burial depth (BD) below seafloor and include clay volume (V_{cl}), P-wave velocity (V_p), and brine saturation (S_b). Note the shift in velocity depth trends (black arrow, middle subplot), with higher V_p in Barents Sea well relative to the North Sea well. This is caused by the large Cenozoic uplift in the Barents Sea, whereas the North Sea represents more or less a continuously subsiding basin except a moderate Miocene tilt and some recent postglacial rebound.

[1]Norwegian University of Science and Technology.
[2]Tullow Oil.
[3]Lehocki Geospace.

http://dx.doi.org/10.1190/tle35040936.1.

burial depth. The porosity as a function of burial depth can be expressed with the following exponential decay function:

$$\phi(Z) = \phi_0 \exp(-cZ), \quad (1)$$

where ϕ is the porosity at burial depth Z, ϕ_0 is the depositional (i.e., critical) porosity at the sea floor (Z = 0), and c is the exponential decay constant. Both ϕ_0 and c will vary depending on lithology, sorting, and clay content. For clean sands, we assume $\phi_0 = 0.4$ (or slightly lower if we want to account for sorting) and $c = 0.13$. The depositional porosity of shales can vary a lot depending on silt content, clay mineralogy, and water salinity. For the Barents Sea shales, we have used a lower depositional porosity (0.3) compared to the North Sea shales (0.45), as the shallow marine Cretaceous shales of the Barents Sea tend to be more silty and marly than the more open marine Tertiary shales in the North Sea. For the Alvheim and Skalle shales, we have used $c = 0.45$. We assume hydrostatic pressure and normal compaction for both sands and shales, yet overpressure may be included in the modeling as porosity reduction can be expressed in terms of effective stress instead of burial depth (e.g., Lander and Walderhaug, 1999).

Next, we model the quartz cementation for the sandstone layers that are buried at temperatures (T) high enough for cementation to occur (i.e., T > 70°C). We need to know the temperature history during geologic time in order to model quartz cementation. In addition, parameters like grain size and amount of clay coating will affect the degree of cementation. The quartz cementation is given by the following equation, which is an analytical solution of a time integral (Walderhaug, 1996):

$$V_{cem} = \phi_{0cc}\left\{1 - \exp\left[-\frac{MaA_0}{\rho\phi_{0cc}bCln10}\left(10^{bT_2} - 10^{bT1}\right)\right]\right\}. \quad (2)$$

V_{cem} is the amount of quartz cement (cm^3) precipitated within a given time interval, and ϕ_{0cc} is the porosity at the start of cementation. The corresponding temperatures at these two times are T_1 and T_2, respectively. M is the molar mass of quartz (60.09 g/mole), and a and b are constants with units of moles/cm^2 and 1/°C, respectively. We use the estimates by Walderhaug (1996), where $a = 1.98 \times 10^{-22}$ and $b = 0.022$. A_0 is the initial quartz surface area expressed in cm^2. Finally, C is the heating rate (°C/Myr), estimated from temperature gradients and burial history curves for different stratigraphic intervals. In the modeling, we assume that mechanical compaction continues after start of cementation, although in reality we may expect cementation to retard the mechanical compaction.

For shales, we take into account the transition from smectite to illite, also a chemical process starting at about 60–70°C. Quartz is a byproduct of this process and can contribute to further stiffening and lithification of illite-rich shales (Avseth et al., 2008) as well as representing an external source of quartz cement in embedded sandstones. However, we only model the effect of mineralogy change in the rock-physics modeling, not the stiffening effect of the cement in shales, as this textural effect is very complex and poorly understood.

The burial history curves needed for the compaction modeling are usually input from geologists, for different stratigraphic intervals. These are standard inputs to basin modeling for evaluation of petroleum systems. In this study, we use these to constrain our rock-physics and AVO modeling. Burial curves also can be estimated or adjusted by fitting our modeled rock-physics depth trends to observed porosity and velocity logs.

Figure 2 shows the compaction modeling for the Alvheim and Skalle wells, respectively. For the Alvheim case, the target reservoir is the Heimdal Fm of Paleocene age (60 Myr), and is today buried at almost 1900 m below the seafloor. The burial history of this layer is represented by the blue curves in the leftmost subplot in Figure 2a, one for the top of the Heimdal Fm and one for the base of the same unit. To explain the observed porosity (ϕ) and velocity trends, we estimate an uplift of only 200 m, which is expected due to Miocene tilting and Quaternary glacial rebound (Avseth et al., 2014). From the Walderhaug modeling, we predict V_{cem} to vary between 3% and 6% and ϕ to vary between 28% and 22% from top to base of Heimdal Fm, which is in good agreement with thin-section analysis and rock-physics diagnostics (Avseth et al., 2009).

For the Skalle case, the target reservoirs are Kolmule Fm and Stø Fm. The burial history for this case involves much more

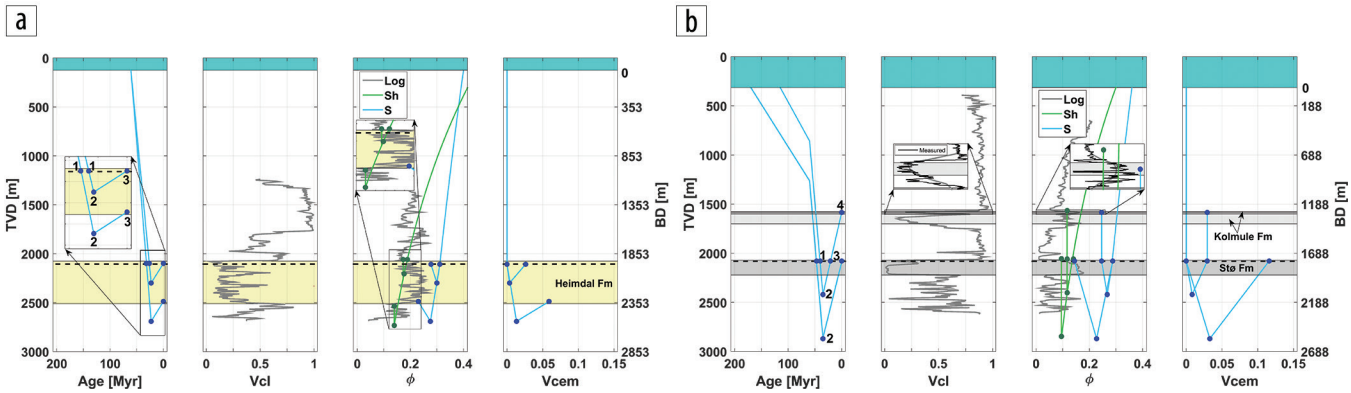

Figure 2. Compaction modeling of reservoirs and cap-rock shales in (a) Alvheim and (b) Skalle wells. The burial history curves to the left are input to the modeling. Porosity (ϕ in third subplot) and cement volume (V_{cem} in fourth subplot) are for sandstones (S, blue curves) modeled by combining empirical porosity-depth trends (T < 70°C) and Walderhaug quartz cementation model (T > 70°C). Note that cement volume increases both during subsidence and uplift as long as temperatures are exceeding 70°C (dashed horizontal line). Key sandstone layers are indicated for both wells. The green porosity (ϕ) curve represents shale (Sh) and is modeled using an empirical porosity-depth trend for the whole interval and is irreversible during uplift. The blue upper layer represents the seawater.

dramatic uplift than in the Alvheim case, as shown in the leftmost sublot of Figure 2b where the two curves represent the tops of the two target reservoirs. To match the porosity and velocity trends in the sandstone intervals, we need to assume an uplift of 800 m, significantly larger than in the Alvheim case. For the Kolmule sandstone, we estimate V_{cem} to be 3% corresponding to ϕ of 24%, whereas V_{cem} in the Stø Fm is found to be around 11% corresponding to ϕ of 14%. The modeled porosities are representative for a well-sorted end member of the sands, and in both Alvheim and Skalle wells, the observed porosities are occasionally lower due to sorting variability. Nevertheless, the compaction modeling described here provides what we assume is expected rock texture for sandstones (porosity and cement volume) and shales (porosity) for a given burial history that will be used as input in the rock-physics modeling in the next step.

Step 2: Rock-physics modeling. Based on the compaction modeling (porosity and cement volume for sandstone; porosity for shale), we can model rock-physics and seismic properties of sandstones with different types of pore fluids. We use Hertz-Mindlin contact theory for unconsolidated sands and Dvorkin-Nur contact cement model for cemented sandstones (Avseth et al., 2005) combined with Gassmann fluid substitution. We assume the mineralogy to be 100% quartz for all the sandstones. A shear weakening factor is applied to account for grain heterogeneity and associated stress relaxations not governed by the contact theory models (Bachrach and Avseth, 2008) in order to obtain realistic V_P/V_S ratios. We also model the rock-physics properties of shales as a function of burial history. We use Hertz-Mindlin contact theory for both the smectite-rich and the illite-rich shales. One can debate the applicability of this theory for shales, as it assumes an isotropic pack of spherical grains. However, using the coordination number as a fitting parameter, we find that a model based on this theory also can be useful for shales. Alternatively, one can apply an inclusion-based model for the shale depth trends (see Avseth et al., 2008). Also for shales, it is important to note that the mechanically compacted porosity will not be reversible during uplift, whereas the effective pressure will be. Hence, shale velocities will decrease slightly during uplift, even when the porosities stay constant.

Figure 3 shows the modeled brine-saturated sand and shale velocities, impedances, and V_P/V_S for the Alvheim and Skalle cases, superimposed on well-log data where the hydrocarbon intervals have been fluid substituted to brine. As we see, the seismic properties predicted based on the compaction modeling fit quite nicely with the well-log observations for both cases. (The well-log data have been upscaled with 5 m blocking, including Backus averaging of V_P and V_S, then resampled. Finally, a simple running average was applied to smooth the logs). V_P/V_S tends to be underestimated for the more heterogeneous sandstone intervals because we assume clean sandstone in the modeling. This is because presence of clay in the sandstone intervals will weaken the shear stiffnesses and significantly increase V_P/V_S.

The observed properties of water-saturated sandstone can be explained only by the presence of quartz cement. There is a significant break in the modeled velocity-depth gradient as the rocks are becoming cemented. The velocities and impedances continue to increase significantly both during subsidence and uplift as long as the rocks are buried at temperatures higher than 70°C, indicated by the dashed horizontal line. Correspondingly, the V_P/V_S decreases significantly because of the increasing cement volume.

Also, the shale trends show abrupt changes across the 70°C threshold, as we model a change from smectite-rich to illite-rich shales at this temperature. Note that the shales can have varying silt content related to both depositional environment and burial depth. We assume quartz content of shales to be relatively low in the mechanical compaction domain, but somewhat higher in the Barents Sea than in the North Sea. For both cases, quartz content increases in the chemical compaction domain since quartz is a byproduct of the smectite-to-illite transition. However, we ignore the textural effect of cementation in shales, which could stiffen the shales further. Still, we capture the shale trends quite nicely. Shales are abundant, and therefore it is relatively easy to obtain good calibration of their trends. However, it sometimes can be challenging to discriminate the effect of uplift from the effect of mineralogy.

Step 3: AVO modeling. Proceeding from the rock-physics modeling of sandstones and shales, we can model expected AVO signatures for sand intervals embedded in shales for a given burial history, using Zoeppritz's equations or linear

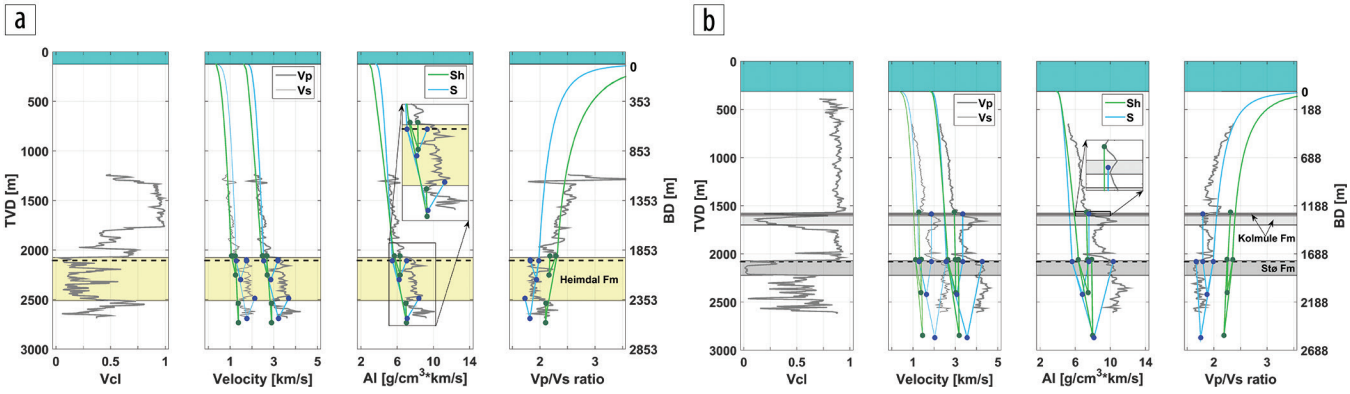

Figure 3. Rock-physics modeling of reservoirs in (a) Alvheim and (b) Skalle wells. We observe a good match between models and well-log data when we assume 200 m uplift in the Alvheim field and 800 m uplift in the Skalle well. Green curves are the modeled cap rock shale trends. (Well logs have been upscaled using a Backus averaging with blocking window of 5 m.)

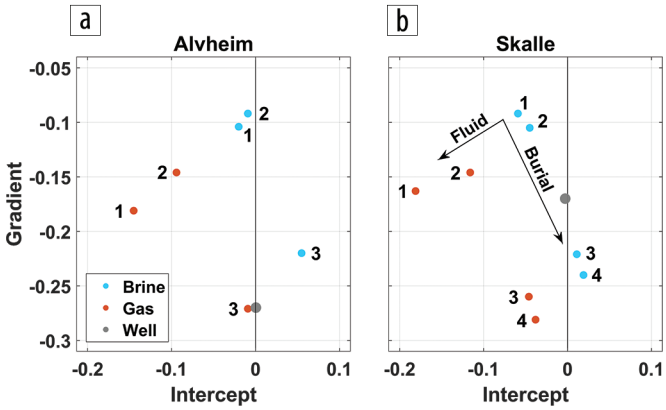

Figure 4. AVO modeling of (a) top Heimdal Fm sst, Alvheim Field and (b) top Kolmule Fm sst, Skalle Field, using the modeled facies depth trends. Blue points are water saturated, red points are gas-saturated sandstones. Reflectivities from upscaled logs in the two wells are superimposed, and we see a very good match in the Alvheim case, but a fair match in the Skalle case. The latter is related to the heterogeneity in the Kolmule sandstone, whereas the modeling assumes clean sandstone.

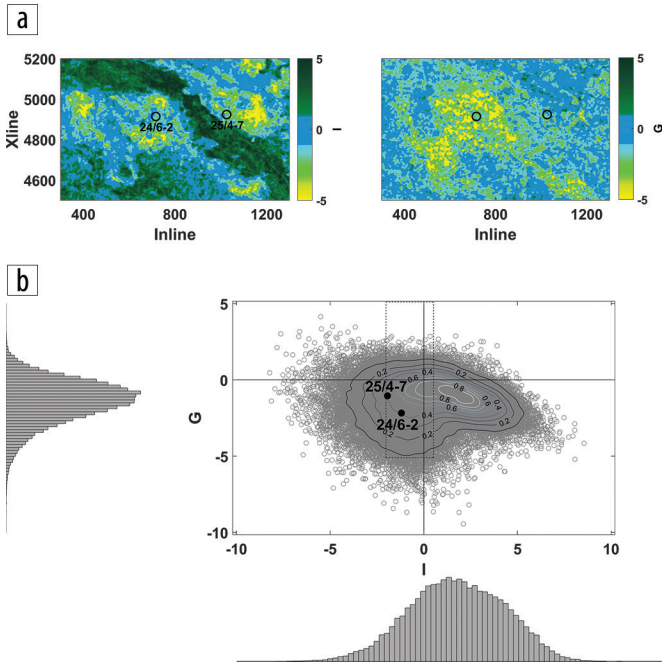

Figure 5. (a) Horizon maps of uncalibrated AVO intercept (I) and gradient (G) in the Alvheim area. (b) Crossplot of I and G, with marginal distributions shown along the axes. A normalized kernel density estimate (NKDE) showing the statistical distribution of the majority of the data is superimposed as contours (Lehocki et al., 2015). The attribute values at the well locations (i.e., nearest CDP) for two wells in the area are indicated.

approximations of Zoeppritz. This can be a very useful exercise in areas with complex geology and few wells where it is not straightforward to extrapolate seismic properties away from well-log observations. Figure 4 shows the AVO modeling of gradient versus intercept for top Heimdal Fm in the Alvheim Field, and for the top Kolmule Fm sandstone in the Skalle discovery, where we picked the V_P, V_S, and density values from the modeled facies depth trends. The numbers and arrows indicate the effect of compaction and cementation with increasing burial combined with the fluid effect, and the highest number represents the present day situation for the Alvheim and Skalle cases, c.f. Figure 2. We see that for the Alvheim case we expect a class II AVO for gas-saturated sandstones capped by shale, whereas for the Skalle case, we expect a class III AVO response. This difference in AVO signature is interesting, given that the Kolmule sandstones in the Skalle Field have similar cement volume (3%) as the upper part of the Heimdal sandstones in the Alvheim Field. This difference in expected AVO signatures is related to the stiffer cap rock shale in the Skalle case and demonstrates how important it is to include the correct shale trends.

The modeled AVO signature fits nicely with the reflectivities estimated from upscaled logs for the Alvheim case. However, for the Skalle case, the well-log-derived gradient is significantly weaker than what is predicted from the burial trends. This is expected since the Kolmule sandstone in the Skalle well is relatively heterogeneous, whereas the modeling assumes clean sandstone. Also, we have assumed 80% patchy gas saturation in the modeling, whereas the Kolmule sandstones have about 35% gas saturation. By linking burial history and rock physics, we are able to predict the expected signature of clean sandstone, even if the well in the area encountered a heterogeneous sandstone interval. This information is essential for the AVO classification and reservoir prediction away from the well.

AVO classification constrained by burial history

Based on rock-physics depth trends defined above and Monte Carlo simulation of depositional variability not accounted for by the rock-physics modeling (e.g., sorting), we can create AVO PDFs of different reservoir facies/fluids at a given depth to be used in AVO classification of intercept and gradient attributes. This is the same procedure as presented by Avseth et al. (2003). However, with the established link between burial history and rock-physics modeling, we now can include diagenesis and tectonic uplift in the AVO modeling. We demonstrate this approach on the Alvheim Field in the North Sea and on the Skalle Field in the Barents Sea.

Case 1: Alvheim Field, North Sea

The Alvheim Field is located in the North Sea and represents a Paleocene oil and gas field. Several publications have demonstrated how AVO can be used to predict hydrocarbon-filled sands in this field (Avseth et al., 2008; Avseth et al., 2009; Rimstad et al., 2012; Lehocki et al., 2015). Figure 5 shows AVO attributes including (uncalibrated) intercept (I) and gradient (G), and the crossplot of these. Intercept and gradient have been estimated from seismic angle stacks. The well used in the compaction and rock-physics modeling in Figures 2 and 3 is annotated in the attribute maps (24/6-2), together with another well in the area (25/4-7). In the AVO crossplot in Figure 5, we show the G versus I values at these two well locations. We observe a class III AVO anomaly at both well locations, which is different from the class II predicted from the burial trends in Figure 4. However, the Monte Carlo simulation will account for depositional variability for a given facies that can yield more than one AVO class. As shown below, we also had to define more than one type of sandstone facies for the Alvheim field.

The next step is to perform classification of the AVO data in Figure 5. Training data are generated based on the depth trends modeled above. The Heimdal Fm reservoir sands are presently located at burial depths of about 1900–2000 m, and the temperatures are close to the onset temperature for quartz cementation. As shown above, maximum burial has probably been a couple of hundred meters deeper than today, as we find the Heimdal Fm to be slightly cemented (3–6%). However, as reported by Avseth et al. (2009), some of the sands in the area are found to be uncemented, whether this is related to small lateral changes in burial history or to some factors inhibiting quartz cementation (e.g., early oil migration, clay coating, heterogeneity, etc.). Therefore, in the classification we include training data for unconsolidated sands (at ca. 20MPa effective pressure) as well as cemented sandstones.

Figure 6a shows the crossplot of calibrated AVO intercept and gradient, with the training data of different lithology and fluids superimposed. The AVO data can be calibrated using the workflow presented by Avseth et al. (2003), where the background cloud in the AVO data is matched with a modeled background cloud using a covariance match. However, in this case we calibrate the AVO data using scalers estimated from upscaled well-log data. The training data are represented by ellipses that correspond to 68% isoprobability contours of a given litho/fluid class (i.e., 68% of simulated data of a given class plots inside the corresponding ellipse). The centers of the ellipses represent the reflectivities predicted from the rock-physics depth trends.

Applying a linear classifier, AVO classification results of pore fluids and facies are obtained in Figure 6b (a spatial median filter is used to smooth the maps). Here we see that the area around well 24/6-2 is classified as most likely gas sandstone and that most of the reservoir sands are classified as cemented. At the neighboring structure, around well 25/4-7, the classification shows most likely oil, and the reservoir sands are classified as more unconsolidated. This fits with the observations at the well locations (see Avseth et al., 2009). Well 24/6-2, which is used in the analysis above, encountered a thick gas column above a thin oil column, whereas well 25/4-7 encountered only oil in a reservoir where the uppermost part of it was found to be unconsolidated. The area around well 24/6-2 likely has been buried slightly deeper than the area around well 25/4-7, and this can explain the distribution of the cemented sandstone facies in Figure 6b. Alternatively, the presence of oil in well 25/4-7 could have inhibited the onset of cement in a local lobe structure (for more detailed discussions, see Avseth et al., 2009).

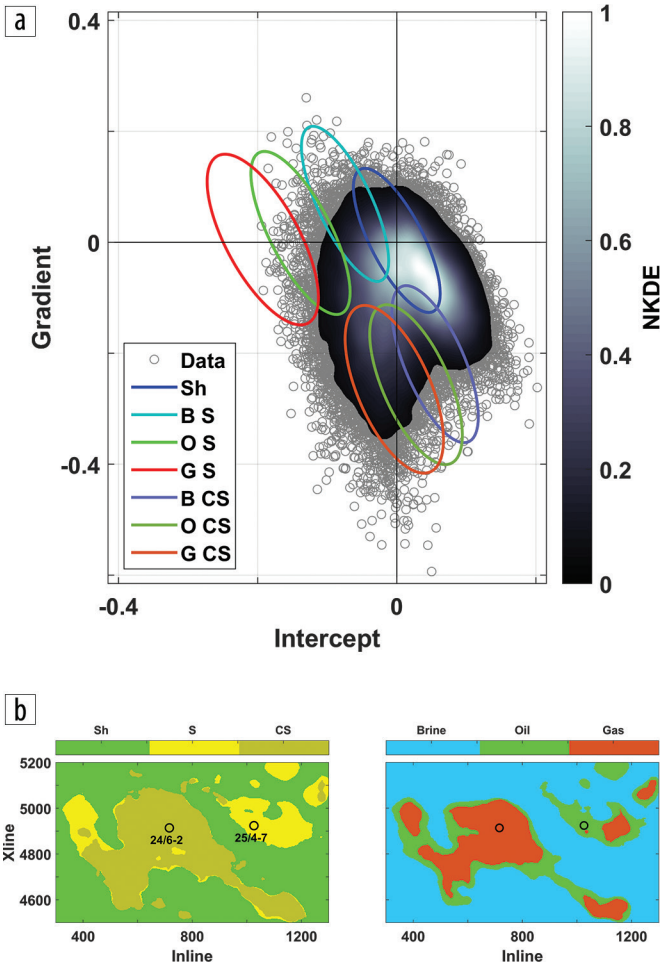

Figure 6. (a) Crossplot of calibrated AVO intercept and gradient (data samples in gray circles, data PDF in shaded colors), with superimposed ellipses representing isoprobability contours (68%) of training data (Sh = shale, B = brine, O = oil, G = gas, S = unconsolidated sand, CS = cemented sandstone). (b) AVO classification results, including lithofacies (left) and pore fluids (right).

Case 2: Skalle discovery, Barents Sea

The Skalle discovery is located just south of the Loppa High in the Barents Sea and represents a Mid Jurassic to Lower Cretaceous gas discovery. In the AVO analysis, we focus on the Lower Cretaceous Kolmule Fm, where subcommercial gas saturation was encountered in a heterogeneous sand. Figure 7 shows AVO attributes including (uncalibrated) intercept and gradient, and

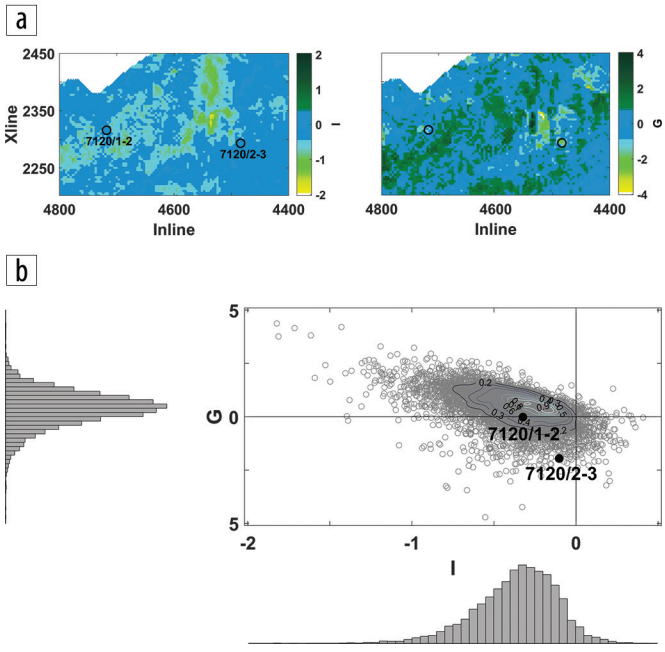

Figure 7. (a) Horizon maps of uncalibrated AVO intercept (I) and gradient (G) in the Skalle area. (b) Crossplot of I and G.

the crossplot of these. The well used in the compaction and rock-physics modeling in Figures 2 and 3 is annotated in the attribute maps (7120/2-3), together with a nearby well that encountered oil shows in a silty shale Kolmule Fm (7120/1-2). The intercept is quite weak, but the gradient map shows a negative anomaly in the area around the Skalle well. Hence, an AVO class II anomaly is observed, which is similar to what we model based on the well-log data (Figure 4). However, as we demonstrated in Figure 4, clean cemented sandstone filled with gas should show a class III AVO in this area.

The reservoir has been buried 800 m deeper than the present day, and is found to be slightly cemented. The maximum burial depth of the Kolmule Fm sandstone then has been just exceeding 2000 m, which is similar to the maximum burial of the uppermost Heimdal Fm sandstone in the Alvheim Field. Hence, given uncertainties in the temperature gradient, we could have a situation where the Kolmule sandstones in the Skalle well have just barely entered the cementation window, and, therefore, we may expect some of the reservoir sands in the area to be uncemented. Thus, we include both cemented sandstone and unconsolidated sands in the classification also in this case. Figure 8a shows the crossplot of calibrated AVO intercept and gradient data, with the training data of different lithology and fluids superimposed. The facies and fluid classification results are shown in Figure 8b, and we see that the Skalle well is located at the pinch out of a sand body saturated with gas. Clean cemented sandstone is predicted at the Skalle well, whereas uncemented sands are predicted just north of the well. Shale is correctly predicted at the neighboring well, 7120/1-2.

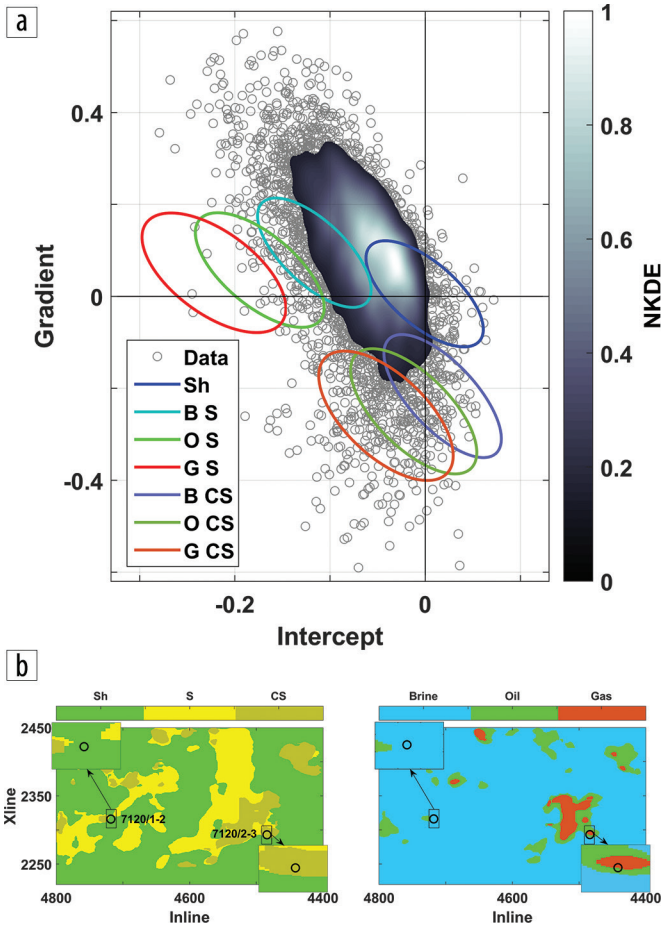

Figure 8. (a) Crossplot of calibrated AVO intercept and gradient (data samples in gray circles, data PDF in shaded colors), with superimposed ellipses representing isoprobability contours (68%) of training data (Sh = shale, B = brine, O = oil, G = gas, CS = cemented sandstone, S = unconsolidated sands). (b) AVO classification results, including lithofacies (left) and pore fluids (right).

Conclusions

We have demonstrated how burial history and modeling of compaction and diagenesis can be combined with rock-physics modeling to predict expected AVO signatures for a given reservoir. This method can be used in a forward-modeling way to predict seismic signatures, given a known burial history. However, it also can be used in an inverse way to predict maximum burial and net erosion, given observed seismic velocities. In this study, the focus has been to create AVO training data that can be used in lithofacies/fluid classification of AVO attributes using the link between burial history and rock physics. The method has been demonstrated on two hydrocarbon discoveries in the North Sea and Barents Sea. Based on the depth trends generated from the combined burial history and rock-physics modeling, we successfully predict the presence of reservoir sands and hydrocarbon saturation in both fields. The method can be used during exploration and prospect screening in areas with limited well control and away from well observations by honoring local burial and tectonic history. The depth trends generated from burial history can also be used to generate low-frequency constraints for simultaneous AVO inversion. TLE

Acknowledgments

We are thankful to operator Lundin Norway and partners Petoro, Dea Norge, Tullow Oil Norge, Det Norske Oljeselskap, and Explora Petroleum of license PL438 (Skalle discovery) on the Norwegian Shelf, and operator Det Norske Oljeselskap and partners ConocoPhillips Scandinavia and Lundin Norway of license PL203 (Alvheim Field) for providing us with the AVO data used in this study.

Corresponding author: Per.Avseth@tullowoil.com

References

Avseth, P., T. Veggeland, and I. Lehocki, 2014, Combined burial history and rock physics modeling of quartz-rich sandstones — Norwegian Shelf demonstrations: 84th Annual International Meeting, SEG, Extended Abstracts, 2809–2813, http://dx.doi.org/10.1190/segam2014-1676.1.

Avseth, P., A. Jørstad, A.-J. van Wijngaarden, and G. Mavko, 2009, Rock physics estimation of cement volume, sorting, and net-to-gross in North Sea sandstones: The Leading Edge, **28**, no. 1, 98–108, http://dx.doi.org/10.1190/1.3064154.

Avseth, P., A. Dræge, A.-J. van Wijngaarden, T. A. Johansen, and A. Jørstad, 2008, Shale rock physics and implications for AVO analysis: A North Sea demonstration: The Leading Edge, **27**, no. 6, 788–797, http://dx.doi.org/10.1190/1.2944164.

Avseth, P., T. Mukerji, and G. Mavko, 2005, Quantitative seismic interpretation — Applying rock physics tools to reduce interpretation risk: Cambridge University Press.

Avseth, P., H. Flesche, and A.-J. van Wijngaarden, 2003, AVO classification of lithology and pore fluids constrained by rock physics depth trends: The Leading Edge, **22**, no. 10, 1004–1011, http://dx.doi.org/10.1190/1.1623641.

Bachrach, R., and P. Avseth, 2008, Rock physics modeling of unconsolidated sands: Accounting for nonuniform contacts and heterogeneous stress fields in the effective media approximation with applications to hydrocarbon exploration: Geophysics, **73**, no. 6, E197–E209, http://dx.doi.org/10.1190/1.2985821.

Brevik, I., A. Callejon, P. Kahn, P. Janak, and D. Ebrom, 2011, Rock physicists step out of the well location, meet geophysicists and geologists to add value in exploration analysis: The Leading Edge, **30**, no. 12, 1382–1391, http://dx.doi.org/10.1190/1.3672483.

Dræge, A., K. Duffaut, T. Wiik, and K. Hokstad, 2014, Linking rock physics and basin history — Filling gaps between wells in frontier basins: The Leading Edge, **33**, no. 3, 240–246, http://dx.doi.org/10.1190/tle33030240.1.

Dvorkin, J., and A. Nur, 1996, Elasticity of high-porosity sandstones: Theory for two North Sea data sets: Geophysics, **61**, no. 5, 1363–1370, http://dx.doi.org/10.1190/1.1444059.

Helset, H. M., J. C. Matthews, P. Avseth, and A-J.van Wijngaarden, 2004, Combined diagenetic and rock physics modeling for improved control on seismic depth trends: 66th Conference and Exhibition, EAGE, Extended Abstracts, F041.

Lander, R., and O. Walderhaug, 1999, Predicting porosity through simulating sandstone compaction and quartz: AAPG Bulletin, **83**, no. 3, 433–449.

Lehocki, I., P. Avseth, and V. Hadžiavdić, 2015, Probabilistic estimation of density and shear information from Zoeppritz's equation: The Leading Edge, **34**, no. 9, 1036–1047, http://dx.doi.org/10.1190/tle34091036.1.

Rimstad, K., P. Avseth, and H. Omre, 2012, Hierarchical Bayesian lithology/fluid prediction: A North Sea case study: Geophysics, **77**, no. 2, B69–B85, http://dx.doi.org/10.1190/geo2011-0202.1.

Walderhaug, O., 1996, Kinetic modeling of quartz cementation and porosity loss in deeply buried sandstone reservoirs: AAPG Bulletin, **80**, no. 5, 731–745, http://dx.doi.org/10.1306/64ED88A4-1724-11D7-8645000102C1865D.